

A BOUNDARY ELEMENT FORMULATION USING THE SIMPLE METHOD

M. M. GRIGOR'EV

Department of Mechanical Engineering, Chemical Technology Institute of Kazan, K. Marx Street 68, Kazan, 420015, Russia

SUMMARY

A new boundary element method is described for calculation of the steady incompressible laminar flows. The method is based on the well-known SIMPLE algorithm. The new boundary element method allows one to find the fields of the pressure and velocity corrections without inner iterations, thus reducing the computational time drastically. This makes it different from the method developed by Patankar and Spalding.³² However, the new method demands a much larger computer storage. The boundary integral equations are discretized with the help of constant boundary elements and constant cells. The values of the integrals along the boundary elements and the cells for the two-dimensional domain are found analytically. To preserve the stability in the iteration process, under-relaxation for the convection terms is used. This paper gives the results of calculations of the flows between two plane parallel plates at $Re = 20$ and $Re = 200$, the flows in a square cavity with a moving upper lid at $Re = 1$ and $Re = 100$ and the flow in a plane channel with sudden symmetric expansion at $Re = 46.6$.

KEY WORDS Boundary integral equation Boundary element method SIMPLE algorithm Two-dimensional laminar flow

INTRODUCTION

There has been a growing interest in the applications of the boundary element method (BEM) to the numerical solution of the fluid flow problems. Although for the problems of solid mechanics the boundary element method^{1–4} is well developed and shows advantages in comparison with the Finite Difference Methods (FDM) and Finite Element Methods (FEM), there are no known applications of BEM to the fluid flow problems which show the same advantages. Moreover, the known boundary element method not only surpasses FDM and FEM in effectiveness but also yields them^{5–23} sometimes.

Now there exist rather universal computer programs which are based on FDM and FEM such as TEACH,²⁴ FIDAP,²⁵ etc. However, there are no universal algorithms and programs based on BEM which are capable of solving both laminar and turbulent flow problems. It seems that they will appear in the near future. Potentially, they must overcome the same programs based on FDM and FEM.

The papers of Wu and Wahbah⁵ and Wu and Thomson⁶ may be considered to be the beginning of the application of the boundary integral equations method to the solution of the problem of viscous incompressible fluid flow. Green's theorem for vectors has given these authors the opportunity to obtain Boundary Integral Equation (BIE), which permits one to determine the velocity field with the help of the vorticity field. Although this approach, which uses the equation

of the vorticity transport, allowed one to eliminate the consideration of the pressure, serious difficulties appeared in determining just the vorticity field itself, which is mainly connected with the formulation of the boundary conditions for the vortex. A reasonable compromise seems to be found by the authors in solving the vortex equation by FDM and formulating the boundary conditions using Taylor series expansion. Correspondingly, the difficulties in the implementation of this 'hybrid' method are the same as those in the implementation of FDM. Further development of this method brought the authors to the 'zonal-hybrid' procedure,^{26,27} permitting them to eliminate the non-viscous domain from the consideration and, thus, to make the calculations effectivity essentially higher.

The impossibility of obtaining BIE from the vorticity transport equation using Green's theorem for the vectors has forced the development of BEM for the variables velocity, vorticity and pressure.⁹⁻¹³ This method was successfully used for laminar incompressible flow calculations⁹⁻¹³ and, recently, was modified for turbulent flow calculations.²⁸ The problems of the correct formulation of the boundary conditions for vortex and the application of this method for compressible flows seem to be the main difficulties in the application of this method.

Utilization of the governing equations which have been written with respect to the variables stream function and vorticity allows one to create the methods for two-dimensional flows in which the pressure has not been considered.^{14,15,21,22} But the possibility of the application of these approaches to three-dimensional flows faces difficulties in obtaining the three-dimensional fluid flow equations in the variables stream function and vorticity.

The most prospective way is to formulate universal methods of calculating the flows on the basis of BEM, using the equations in the natural variables, velocity and pressure. Here the main difficulty is to determine the pressure. So, for the beginning it may be useful to utilize the ideas of determining the pressure which were used earlier both for FDM and FEM.

The penalty method for BEM has been used widely and successfully by Kitagawa *et al.*¹⁶⁻¹⁸ and Kitagawa.¹⁹ They used it for calculating the two-dimensional flows with natural and forced convection. It also seems possible to generalize this method for more complicated flows.

The advantages of BEM in comparison with other methods could be seen in the solution of Stokes' problem,^{29,30} when the inertia forces are negligible in comparison with the viscous forces. In this case the linear problem with the use of the special fundamental solutions has been converted to the system of BIEs only for the boundary values.³¹ The discretization of the BIE by boundary elements gives a system of linear algebraic equations which can be solved by the Gauss elimination method. The utilization of the BEM technique for Stokes' problem allows one to decrease the dimension of the problem on the whole, essentially decreasing the necessary computer storage and the time of program implementation; it also allows one to solve the problem without iterations.

However, the non-linearity of the Navier-Stokes equations practically does not permit one to realize the potential advantages of BEM. Thus, all known methods for solving the Navier-Stokes equations based on BEM yield to the best successful FEM in effectivity.

This paper investigates the BEM formulation of the well-known SIMPLE method which was developed by Patankar and Spalding.³²⁻³⁴ The method was tested for the calculation of steady two-dimensional laminar fluid flows such as: (a) the flow between two plane parallel plates; (b) the flow in a square cavity with a moving upper lid; (c) the flow in a plane channel with sudden symmetric expansion. The results of the calculations are in agreement with the data obtained by other authors.

This method could be easily applied for calculating three-dimensional, turbulent and unsteady flows. Moreover, the method allows one to solve problems for domains of complex configuration without extra difficulties.

Unfortunately, here the BIEs are non-linear; so, they were solved by iteration method using under-relaxation.

Our method is applicable to both two-dimensional and three-dimensional steady laminar incompressible flows. Although the paper considers only two-dimensional domains, the method could be easily modified to three-dimensional domains.

GOVERNING EQUATIONS

The system of the equations for steady laminar incompressible flow for the dimensionless variables in domain Ω has the following tensor form:

$$\frac{\partial u_i}{\partial x_i} = 0, \tag{1}$$

$$u_j \frac{\partial u_i}{\partial x_j} = - \frac{\partial p}{\partial x_i} + \nu \frac{\partial^2 u_i}{\partial x_j \partial x_j}. \tag{2}$$

On the part Γ_1 of the border Γ , the values of the derivatives with respect to outward normal to the border, $W_i = \partial u_i / \partial n$, are given and on the remaining part Γ_2 , the exact values of the velocities u_i are given.

Green's theorem allows one to obtain the boundary integral equation from (2):

$$c(\xi)u_i(\xi) + \int_{\Gamma} u_i \frac{\partial u^*}{\partial n}(\mathbf{x}, \xi) d\Gamma(\mathbf{x}) + \frac{1}{\nu} \int_{\Omega} \left(\frac{\partial p}{\partial x_i} + u_j \frac{\partial u_i}{\partial x_j} \right) u^*(\mathbf{x}, \xi) d\Omega(\mathbf{x}) = \int_{\Gamma} \frac{\partial u_i}{\partial n} u^*(\mathbf{x}, \xi) d\Gamma(\mathbf{x}), \tag{3}$$

where u^* is a fundamental solution of the Laplace equation.³ The velocity derivatives are obtained by differentiation of BIE (3) with respect to ξ_i co-ordinates (for $\xi \notin \Gamma$):

$$\frac{\partial u_i}{\partial \xi_i} + \int_{\Gamma} u_i \frac{\partial q^*}{\partial \xi_i}(\mathbf{x}, \xi) d\Gamma(\mathbf{x}) + \frac{1}{\nu} \int_{\Omega} \left(\frac{\partial p}{\partial x_i} + u_j \frac{\partial u_i}{\partial x_j} \right) \frac{\partial u^*}{\partial \xi_i}(\mathbf{x}, \xi) d\Omega(\mathbf{x}) = \int_{\Gamma} W_i(\mathbf{x}) \frac{\partial u^*}{\partial \xi_i}(\mathbf{x}, \xi) d\Gamma(\mathbf{x}), \tag{4}$$

where $q^* = \partial u^* / \partial n$.

A supplementary equation for determining the pressure can be obtained by reasoning as follows. Assume that we have approximate fields of velocity $u_i^{(0)}$ and pressure $p^{(0)}$. In the general case, the velocity field $u_i^{(0)}$ does not satisfy the continuity equation (1). The problem is to find such a field of pressure p which gives the velocity field from the equation (3), satisfying equation (1). Assume that u'_i, p' are such 'supplements' of the velocity and the pressure, respectively; then the relations

$$u_i = u_i^{(0)} + u'_i, \quad p = p^{(0)} + p' \tag{5}$$

are valid.

We consider all velocity changes to be caused only by the pressure gradient:

$$\frac{\partial u'_i}{\partial t} = - \frac{\partial p'}{\partial x_i}. \tag{6}$$

Integrating (6) with respect to the time variable, we obtain

$$u'_i = - \lambda \frac{\partial p'}{\partial x_i}, \tag{7}$$

where $\lambda = \Delta t$ is the time step and $u'_i = 0$ at $t_0 = 0$. As the velocity field u_i must satisfy the continuity equation (1), then taking into account (5) and (7), we will obtain Poisson's equation for the

pressure correction

$$\frac{\partial^2 p'}{\partial x_j \partial x_j} = \frac{1}{\lambda} \frac{\partial u_i^{(0)}}{\partial x_i}. \quad (8)$$

An investigation of (8) shows that if, on the part Γ_p of the border Γ , $p' = 0$, and, on the part Γ_f , $\partial p' / \partial n = 0$, then for the divergent velocity field

$$\frac{\partial u_i^{(0)}}{\partial x_i} = 0,$$

the pressure correction is zero on the whole domain Ω .

Green's theorem allows one to obtain BIE for the pressure correction from equation (8):

$$c(\xi) p'(\xi) + \int_{\Gamma} p'(\mathbf{x}) \frac{\partial u^*}{\partial n}(\mathbf{x}, \xi) d\Gamma(\mathbf{x}) + \frac{1}{\lambda} \int_{\Omega} \frac{\partial u_i^{(0)}}{\partial x_i} u^*(\mathbf{x}, \xi) d\Omega(\mathbf{x}) = \int_{\Gamma} \frac{\partial p'}{\partial n}(\mathbf{x}) u^*(\mathbf{x}, \xi) d\Gamma(\mathbf{x}). \quad (9)$$

Taking into account (7) we rewrite the derivative of pressure correction with respect to the outward normal to the border in the form

$$\frac{\partial p'}{\partial n} = -\frac{f'}{\lambda}, \quad (10)$$

where $f' = u'_i n_i$ is the velocity correction orthogonal to the border. Finally, the BIE (9) takes the following form:

$$c(\xi) p'(\xi) + \int_{\Gamma} p'(\mathbf{x}) q^*(\mathbf{x}, \xi) d\Gamma(\mathbf{x}) + \frac{1}{\lambda} \int_{\Omega} \frac{\partial u_i^{(0)}}{\partial x_i} u^*(\mathbf{x}, \xi) d\Omega(\mathbf{x}) + \frac{1}{\lambda} \int_{\Gamma} f'(\mathbf{x}) u^*(\mathbf{x}, \xi) d\Gamma(\mathbf{x}) = 0. \quad (11)$$

Differentiating (11) with respect to the ξ_i co-ordinate and taking into account (7), we will obtain BIE for the velocity corrections calculation:

$$u'_i(\xi) = \lambda \int_{\Gamma} p'(\mathbf{x}) \frac{\partial q^*}{\partial \xi_i}(\mathbf{x}, \xi) d\Gamma(\mathbf{x}) + \int_{\Omega} \frac{\partial u_i^{(0)}}{\partial x_i} \frac{\partial u^*}{\partial \xi_i}(\mathbf{x}, \xi) d\Omega(\mathbf{x}) + \int_{\Gamma} f'(\mathbf{x}) \frac{\partial u^*}{\partial \xi_i}(\mathbf{x}, \xi) d\Gamma(\mathbf{x}). \quad (12)$$

BIE discretization by constant boundary elements and cells

We will divide the boundary Γ of domain Ω into N_b constant boundary elements (BE) with the nodes at the centres of BE, and the domain Ω into N_c constant cells with the nodes at cells' geometric centres. The discretization of BIE (3) when the observation point is situated at the centre of BE ($m = 1, 2, \dots, N_b$) gives

$$c_m u_{im} + \sum_{j=1}^{N_b} u_{ij} \hat{H}_{jm} = \sum_{j=1}^{N_b} W_{ij} G_{jm} - \frac{1}{\nu} \sum_{k=1}^{N_c} (K_{ik}^{\Omega} + P_{ik}^{\Omega}) D_{km}. \quad (13)$$

In equation (13) the coefficient $c_m = 0.5$ for all constant BE. The following designation is accepted for integrals according to j BEs and k cells:

$$\hat{H}_{jm} = \int_{\Gamma_j} q^*(\mathbf{x}, \xi) d\Gamma(\mathbf{x}), \quad G_{jm} = \int_{\Gamma_j} u^*(\mathbf{x}, \xi) d\Gamma(\mathbf{x}) \quad (14)$$

$$P_{ik}^{\Omega} = \left(\frac{\partial p}{\partial x_i} \right)_k, \quad K_{ik}^{\Omega} = \left(u_{\alpha} \frac{\partial u_i}{\partial x_{\alpha}} \right)_k, \quad D_{km} = \int_{\Omega_k} u^*(\mathbf{x}, \xi) d\Omega(\mathbf{x}). \quad (15)$$

The discrete BIE (13) could be rewritten in the canonical form for every space co-ordinate $i=1, 2, 3$:

$$\mathbf{Ax} = \mathbf{b}, \quad (16)$$

where \mathbf{x} is the vector of the unknown values. The system of N_b linear algebraic equations for every space co-ordinate has been solved by the Gauss elimination method.

Placing the observation points at the cells' geometric centres ($k=1, 2, \dots, N_c$), one may discretize BIE for the internal nodes velocity calculation $m=1, 2, \dots, N_c$ at $c_m=1$:

$$u_{im}^\Omega = - \sum_{j=1}^{N_b} u_{ij} \hat{H}_{jm}^\Omega + \sum_{j=1}^{N_b} W_{ij} G_{jm}^\Omega - \frac{1}{v} \sum_{k=1}^{N_c} (K_{ik}^\Omega + P_{ik}^\Omega) D_{km}^\Omega, \quad (17)$$

where the following notations are used for $\xi \in \Omega$:

$$\hat{H}_{jm}^\Omega = \int_{\Gamma_j} q^*(\mathbf{x}, \xi) d\Gamma(\mathbf{x}), \quad G_{jm}^\Omega = \int_{\Gamma_j} u^*(\mathbf{x}, \xi) d\Gamma(\mathbf{x}), \quad D_{km} = \int_{\Omega_k} u^*(\mathbf{x}, \xi) d\Omega(\mathbf{x}). \quad (18)$$

In the above-mentioned notations, the upper index Ω denotes that the variable is related to the cell.

The discretization of equation (4) allows one to calculate the velocity derivatives in explicit form by the space co-ordinates $l=1, 2, 3$:

$$\left(\frac{\partial u_i}{\partial \xi_l} \right)_m^\Omega = \sum_{j=1}^{N_b} W_{ij} \gamma_{ijm}^\Omega - \sum_{j=1}^{N_b} u_{ij} \beta_{ijm}^\Omega - \frac{1}{v} \sum_{k=1}^{N_c} (K_{ik}^\Omega + P_{ik}^\Omega) \theta_{ikm}^\Omega, \quad (19)$$

where the notations for the surface

$$\beta_{ijm}^\Omega = \int_{\Gamma_j} \frac{\partial q^*}{\partial \xi_l}(\mathbf{x}, \xi) d\Gamma(\mathbf{x}), \quad \gamma_{ijm}^\Omega = \int_{\Gamma_j} \frac{\partial u^*}{\partial \xi_l}(\mathbf{x}, \xi) d\Gamma(\mathbf{x}) \quad (20)$$

and for the volume integrals

$$\theta_{ikm}^\Omega = \int_{\Omega_k} \frac{\partial u^*}{\partial \xi_l}(\mathbf{x}, \xi) d\Omega(\mathbf{x}) \quad (21)$$

are used.

Discrete BIE for calculating the pressure corrections in boundary and internal nodes have the following form, respectively:

$$0.5 p'_m + \sum_{j=1}^{N_b} p'_j \hat{H}_{jm} + \frac{1}{\lambda} \sum_{j=1}^{N_b} f'_j G_{jm} + \frac{1}{\lambda} \sum_{k=1}^{N_c} S_k^{(0)} D_{km} = 0, \quad (22)$$

$$p'_m = - \sum_{j=1}^{N_b} p'_j \hat{H}_{jm} - \frac{1}{\lambda} \sum_{j=1}^{N_b} f'_j G_{jm} - \frac{1}{\lambda} \sum_{k=1}^{N_c} S_k^{(0)} D_{km}, \quad (23)$$

where the velocity divergence is denoted by

$$S_k^{(0)} = \left(\frac{\partial u_i^{(0)}}{\partial x_i} \right)_k. \quad (24)$$

As the system (22) of BIEs for $m=1, 2, \dots, N_b$ may be rewritten in canonical form (16) and may then be solved by the Gauss elimination method from BIE (23), the values of pressure corrections may be calculated in explicit form at all internal nodes $m=1, 2, \dots, N_c$.

The discretization of BIE (12) allows one to obtain also the formula for calculating the velocity corrections at internal nodes $m=1, 2, \dots, N_c$ in an explicit form:

$$u_{im}^{\Omega} = \lambda \sum_{j=1}^{N_b} p'_j \beta_{ijm}^{\Omega} + \sum_{j=1}^{N_b} f'_j \gamma_{ijm}^{\Omega} + \sum_{k=1}^{N_c} S_k^{(0)} \theta_{ikm}^{\Omega}. \quad (25)$$

For the determination of proper pressure and velocity corrections, it is necessary to establish correct boundary conditions for p' and f' . So, on the Γ_p part of the full boundary Γ , condition $p'=0$ is specified and, on the other part Γ_f , $f'=0$. Usually, the boundary Γ_f is the part where the value of mass flow (the wall, for example) is specified:

$$f = u_i n_i \equiv \text{const}, \quad (26)$$

and the remaining part of the boundary is Γ_p as usual.

Analysing formulae (14), (15), (18), (20) and (21), one can see that surface and volume integrals do not contain velocity and pressure variables, and depend only on the geometric characteristics of the calculating domain. So, using the non-staggered grid, they could be calculated only once and thereafter kept unchanged during further calculations. In the general case, all matrix elements are non-zero and, so, they need much computer storage. The formulae for integral calculations along the boundary elements and the cells for two-dimensional problems are given in Appendix. They may be easily generalized for three-dimensional regions.

SOLUTION PROCEDURE

After discretization of the calculation domain into the boundary elements and volumetrical cells, it is possible to calculate the coefficient matrices for discrete BIEs. For every BE we determine whether it belongs to Γ_1 or Γ_2 , and to Γ_f or Γ_p ; correspondingly, the boundary conditions are determined for W_{ij} or u_{ij} , and f' or p' . By analogy we will specify the initial values P_{ik}^{Ω} and K_{ik}^{Ω} for every cell, usually equal to zero.

Further, the calculations are carried out in the following order:

1. The unknown boundary values of the velocities u_{im} and their derivatives with respect to the outward normal W_{im} are found from (13).
2. The values of the velocities u_{im}^{Ω} are calculated in an explicit form from (17). And the values of their derivatives $(\partial u_i / \partial \xi_i)_m^{\Omega}$ at all internal nodes are calculated from (19).
3. Taking into account that the velocities and their derivatives found above are approximate, the divergence $S_m^{(0)}$ values are found at internal nodes $m=1, 2, \dots, N_c$.
4. The unknown values of the corrections p'_m and f'_m at boundary nodes $m=1, 2, \dots, N_b$ are calculated using equation (22).
5. The pressure and velocity corrections are calculated from (23) and (25) at all internal nodes $m=1, 2, \dots, N_c$.
6. The velocity and pressure corrections at all internal nodes take the form

$$u_{im}^{\Omega} = u_{im}^{(0)\Omega} + u'_{im}, \quad p_m^{\Omega} = p_m^{(0)\Omega} + p'_m, \quad m=1, 2, \dots, N_c,$$

and at boundary nodes of the domain, the form

$$u_{im} = u_{im}^{(0)} + u'_{im}, \quad p_m = p_m^{(0)} + p'_m, \quad m=1, 2, \dots, N_b.$$

Then the convection terms are calculated from the velocities and their derivatives from (15).

To calculate the pressure derivatives of internal nodes, the relation

$$p_{ik}^{\Omega} = P_{ik}^{(0)\Omega} - \frac{u_{ik}^{\Omega}}{\lambda} \tag{27}$$

obtained from (5) and (7) is used.

It must be mentioned that the velocity correction at a boundary node is not necessary as the correction of velocity in a limiting case tends to zero. It is important because their components cannot be determined from the correction f' for BE which are not orthogonal to any of the co-ordinate axes.

7. We check the convergence. If the convergence is not achieved, we return to step 1.

The convergence of the solution was controlled by the maximum value of the increment at all nodal points of the calculation domain:

$$|(u_{im}^{\Omega})_q - (u_{im}^{\Omega})_{q-1}| \leq \delta_i,$$

where q is the iteration number and the velocities values are taken after their correction. The convergence criterion for the main calculations was $\delta_1 = 10^{-4}$ for u_1 component and $\delta_2 = 3 \times 10^{-5}$ for u_2 .

Preliminary calculations have displayed that such a cycle may turn unstable and, so, it is necessary to use under-relaxation for the convection terms

$$K_{ik}^{\Omega} = \alpha(K_{ik}^{\Omega})_q - (\alpha - 1)(K_{ik}^{\Omega})_{q-1}. \tag{28}$$

The initial value of the relaxation coefficient is recommended to be set equal to v (for $v < 1$); then with every iteration it may grow with the coefficient to 1.01–1.02 in a geometric progression. Moreover, the initial value of the coefficient λ in the pressure and velocity correction algorithm one may assume to be equal to $1/v$, which then decays with every iteration in a geometric progression with the coefficient to 0.98–0.99. In this case the calculations show stability and convergence. In the general case, λ value of the coefficient does not influence the final result.

We will give now several useful ideas for implementation of computer programs. First of all, one must check the mass flow conservation on the border of the calculation domain. In the limit case the velocity divergence tends to zero; so, the discretization of the relation

$$\int_{\Omega} \frac{\partial u_i}{\partial x_i} d\Omega = \int_{\Gamma} u_i n_i d\Gamma$$

allows one to control the mass flow conservation on the whole border:

$$\sum_{m=1}^{N_b} (u_{1m} n_{1m} + u_{2m} n_{2m}) L_m = Q. \tag{29}$$

In (29), L_m is the length of the m th BE.

The second suggestion is to check the perfectness of the algorithm by checking the pressure and velocity corrections. As the equality

$$\int_{\Omega} \frac{\partial u'_i}{\partial x_i} d\Omega = \int_{\Gamma} f' d\Gamma$$

must be valid, for divergent velocity field the identity

$$\sum_{k=1}^{N_c} S_k^{(0)} A_k = \sum_{m=1}^{N_b} f'_m L_m$$

must also be valid correspondingly, where A_m is the area of k cells.

The third suggestion is to compare the velocity derivatives evaluated from equation (19) with the ones obtained in any other way (for instance, by the approximation using the method of least squares for the regular domains) from the discretized BIE (17). The velocity corrections which were obtained from BIE (25) may be analogously compared with the ones obtained from (7), where the pressure derivatives were determined by an alternative differencing (usually, velocity derivatives) of the pressure corrections from (23).

It must be mentioned that the inner cycle in the standard SIMPLE algorithm based on the control volume method is not necessary in our algorithm. So, the time of the calculations may be essentially decreased.

VORTICITY AND STREAM FUNCTION CALCULATIONS

After velocity and pressure fields are found, one can determine the vorticity

$$\omega = \frac{\partial u_2}{\partial x_1} - \frac{\partial u_1}{\partial x_2}, \quad (30)$$

and the stream function Ψ for the two-dimensional flow. Taking into account

$$u_1 = \frac{\partial \Psi}{\partial x_2}, \quad u_2 = -\frac{\partial \Psi}{\partial x_1}, \quad (31)$$

we will obtain Poisson's equation for the stream function from (30):

$$\frac{\partial^2 \Psi}{\partial x_j \partial x_j} = -\omega. \quad (32)$$

Using the Green's theorem in equation (32), we obtain BIE

$$c(\xi)\Psi(\xi) + \int_{\Gamma} \Psi(\mathbf{x})q^*(\mathbf{x}, \xi) d\Gamma(\mathbf{x}) = \int_{\Omega} \omega(\mathbf{x})u^*(\mathbf{x}, \xi) d\Omega(\mathbf{x}) + \int_{\Gamma} \frac{\partial \Psi}{\partial n}(\mathbf{x})u^*(\mathbf{x}, \xi) d\Omega(\mathbf{x}), \quad (33)$$

which is discretized to the form

$$0.5\Psi_m + \sum_{j=1}^{N_b} \Psi_j \hat{H}_{jm} = \sum_{j=1}^{N_b} \left(\frac{\partial \Psi}{\partial n} \right)_j G_{jm} + \sum_{k=1}^{N_c} \omega_k^{\Omega} D_{km} \quad (34)$$

for boundary nodes ($m = 1, 2, \dots, N_b$) and

$$\Psi_m^{\Omega} = \sum_{j=1}^{N_b} \left(\frac{\partial \Psi}{\partial n} \right)_j G_{jm}^{\Omega} - \sum_{j=1}^{N_b} \Psi_j \hat{H}_{jm}^{\Omega} + \sum_{k=1}^{N_c} \omega_k^{\Omega} D_{km}^{\Omega} \quad (35)$$

for internal nodes ($m = 1, 2, \dots, N_c$).

The algorithm for determining ω and Ψ is easy and permits one to find them without iterations:

1. The vorticity at internal nodes is found from the known velocity derivatives from (30).
2. The unknown values of the stream functions Ψ_m and their derivatives with respect to the outward normal to the border $(\partial \Psi / \partial n)_m$ are found by the Gauss elimination method from equation (34) rewritten to a canonical form.
3. The stream function values at all internal nodes of the domain Ω are determined from (35) in explicit form.

Although the algorithm of determining the values of Ψ, ω has the auxiliary meaning, the calculation of the vorticity and stream function is an important step in the analysis of the results of problem's numerical solution.

RESULTS

Flow in the inlet section of the parallel plates

The steady incompressible viscous flow was calculated by the above algorithm for two Reynolds numbers $Re=2/\nu$: 20 and 200 and was compared with the known results.³⁵⁻⁴⁰

As the flow is symmetrical, only half of the channel height was considered. The boundary conditions for this problem have the following form:

on the wall the no-slip conditions are specified

$$u_1 = u_2 = 0, \quad \Psi = 0, \quad f' = 0;$$

on the channel axis of symmetry

$$\partial u_1 / \partial n = 0, \quad u_2 = 0, \quad \Psi = 1, \quad f' = 0;$$

on the channel entrance

$$u_1 = 1, \quad u_2 = 0, \quad \Psi = x_2, \quad f' = 0;$$

rather far away from the channel entrance (outflow conditions)

$$\partial u_1 / \partial n = \partial u_2 / \partial n = 0, \quad \partial \Psi / \partial n = 0, \quad p' = 0.$$

The outflow boundary was situated at $x_1 = 3$ and $x_1 = 8$ for Reynolds numbers of 20 and 200, respectively. If for $Re = 20$ such remoteness was enough, in the case with $Re = 200$ the length of the channel was not enough for the formation of the fully developed flow.

The calculation domain for $Re = 20$ was discretized into 60 boundary elements and 450 triangular cells on the uniform mesh. For $Re = 200$ it was discretized for the mesh with exponential thickness along the x_1 axis and was divided into 60 BEs and 400 cells. The personal computer PC/AT 286 was used; so, it was impossible to use a finer mesh. It must be mentioned that, during the numerical implementation of this method, the arrays D_{km}^Ω , θ_{ikm}^Ω which have N_c^2 and $2N_c^2$ elements, respectively, took the main computer storage.

The usual convergence process is displayed in Figure 1. The values of root-mean-square residuals

$$\varepsilon_i = \sqrt{\left\{ \sum_{k=1}^{N_c} [(u_{im}^\Omega)_k - (u_{im}^\Omega)_{k-1}]^2 / N_c \right\}}$$

for velocity u_i decay quickly during the first 10–15 iterations, but then their decay becomes slow. The convergence of the solution procedure ($\delta_1 = 10^{-4}$, $\delta_2 = 3 \times 10^{-5}$) required 127 iterations at $Re = 20$ and 236 iterations at $Re = 200$.

In Figure 2 the change of the mass flow during the iterations before correction Q_1 and after correction Q_2 according to the SIMPLE algorithm on the boundary of the calculation domain for $Re = 200$ is shown. Q_1 decays fast during the first 15 iterations and then changes slowly near zero. For Q_2 the SIMPLE algorithm yields a decay of 8–10 times the discrepancy of the mass flow on the boundary; so, the mass flow Q_2 is practically always equal to zero.

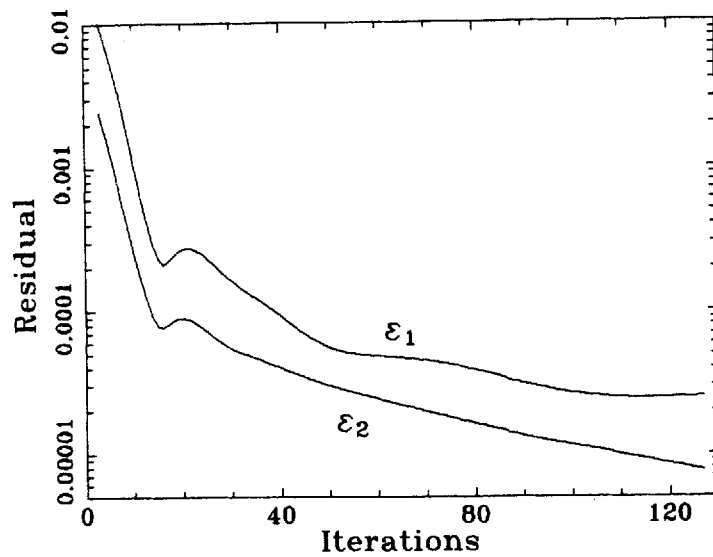


Figure 1. The iteration process convergence of the method for inlet flow between two parallel plates problem at $Re = 20$

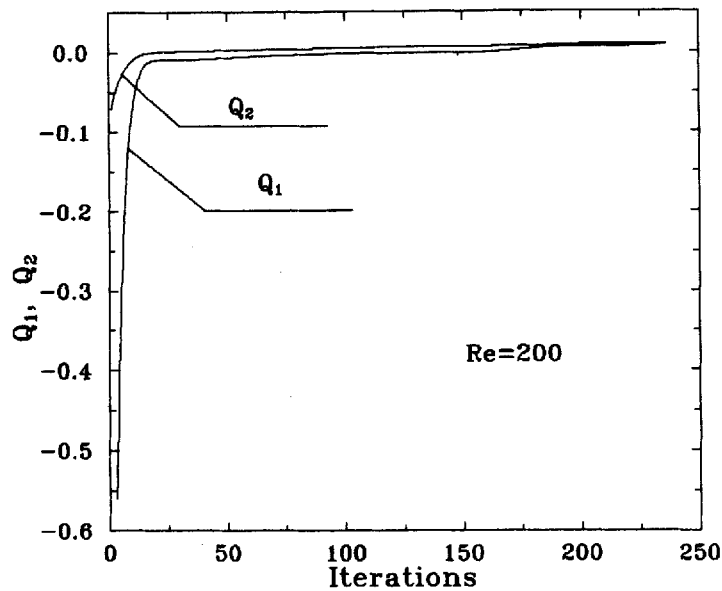


Figure 2. The mass flow changes during the iterations before and after correction

The development of profiles for the longitudinal component of velocity is shown in Figure 3. It must be mentioned that there are convexities in the velocity profiles at the inlet section of their development, both for $Re = 20$ (Figure 3(a)) and for $Re = 200$ (Figure 3(b)). The same situation was mentioned in References 36–40. This development of velocity profiles with negative-gradient zones ($\partial u_1 / \partial x_2 < 0$) was found only under 'hard' inflow boundary conditions, but under 'soft'

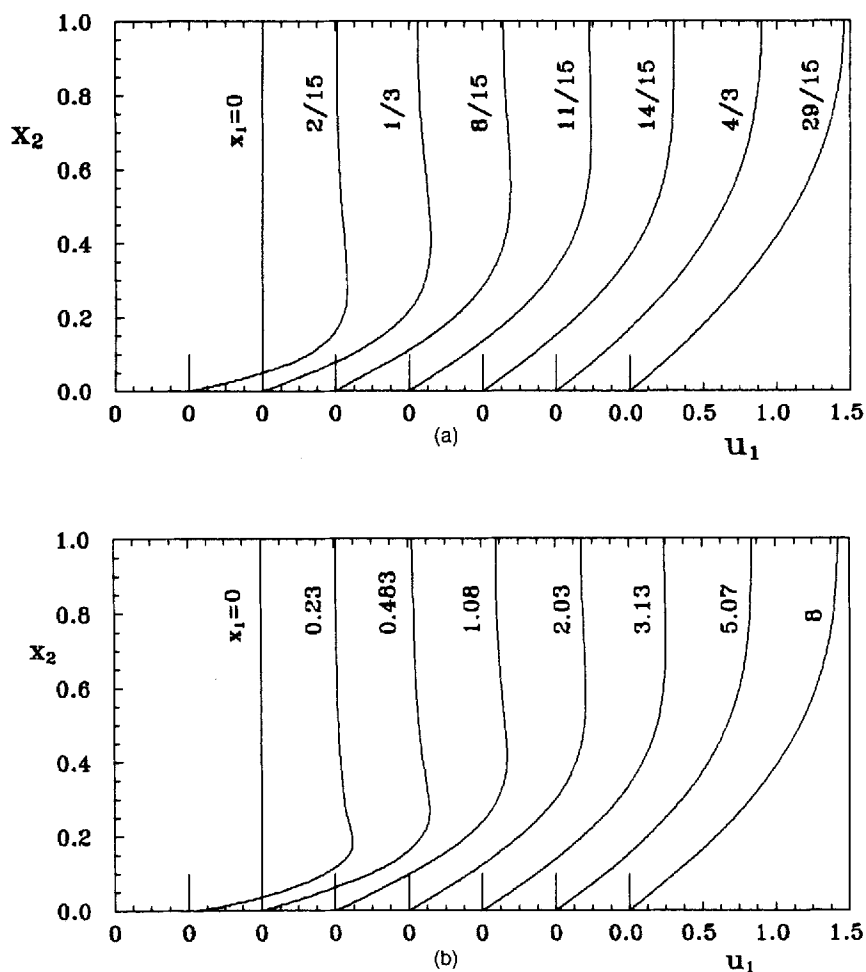


Figure 3. The development of the velocity profiles in the inlet section of channel: (a) $Re=20$; (b) $Re=200$

inflow boundary conditions ($\partial u_2 / \partial n = 0$) the negative-gradient zones were absent. The results obtained earlier in References 35 and 36 testify to this as well.

On the outflow boundary the velocity profiles coincided rather closely with the distribution

$$u_1 = 1.5x_2(2 - x_2)$$

only for $Re=20$, but for $Re=200$ there was a small deviation from the theoretical results because of a too small length of the inlet section (Figure 4).

Figure 5 shows the changes of the velocity's longitudinal component on the channel axis of symmetry. The results obtained by this method were compared with the known data.^{37, 40} It must be mentioned that the results agree well for $Re=20$ though for BEM the coarse mesh was used. A bit worse is the agreement with the results of Morihara and Cheng⁴⁰ and Gillis and Brandt³⁷ for $Re=200$. It is mostly seen approaching the calculation domain outlet. Here the length of the calculation domain was also noticed as being not enough.

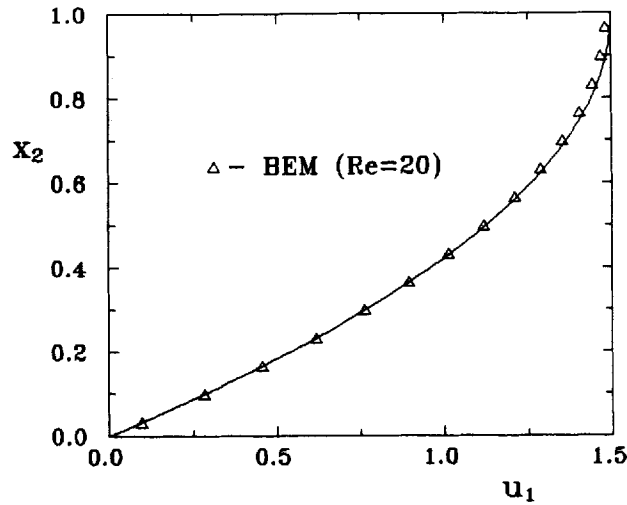


Figure 4. The comparison of the velocity profile at the outlet section of the channel (points) with the developed velocity profile (line)

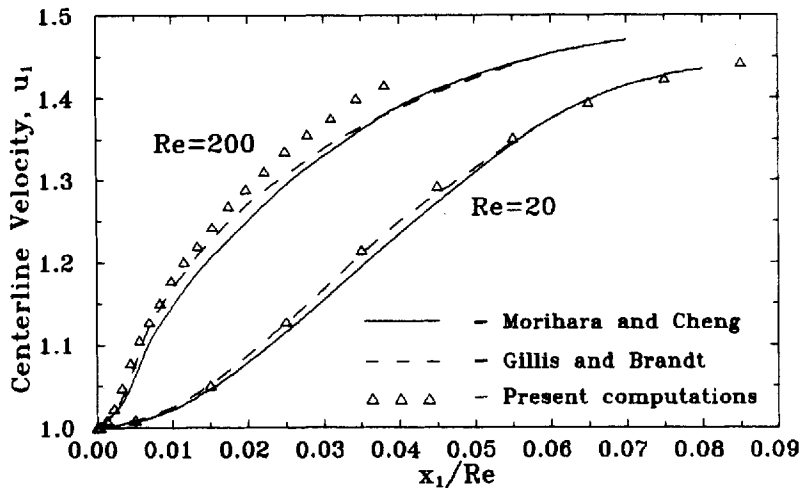


Figure 5. The development of the streamwise velocities on the channel centreline

The streamlines for $Re=20$ and $Re=200$ in Figure 6 have much in common in quality. They curve essentially only on the inflow domain and then become smooth rather quickly. Analogously, the pressure changes essentially along the co-ordinate x_2 only on the inlet section of the flow (Figure 7); then the derivatives $\partial p/\partial x_2$ become too small in comparison with $\partial p/\partial x_1$. On the channel wall the pressure drop becomes stable a bit earlier (Figure 8) than on the axis of symmetry. The analysis of the data in Figures 8 and 9 for $Re=20$ supports the known fact that the pressure drop becomes stable earlier ($x_1=0.75$) than the friction coefficient ($x_1=1.1$). The product $c_f Re$ in this case corresponds to the value of vorticity on the wall ω_w , which is -3 for the steady

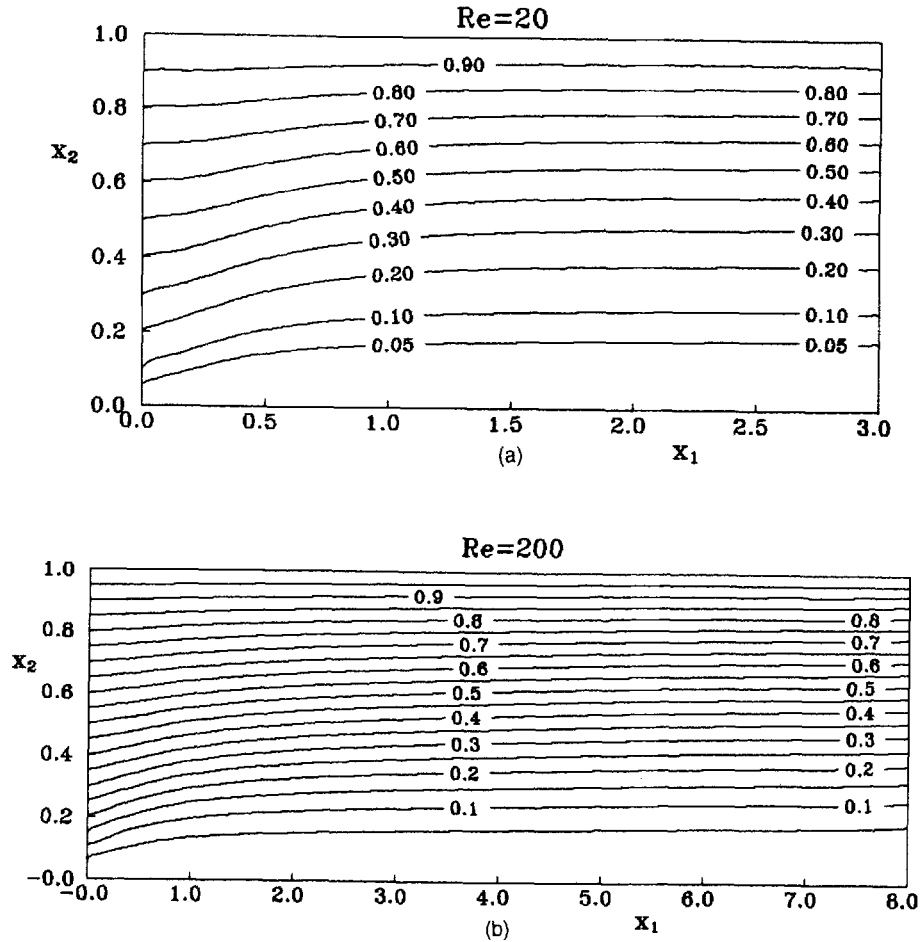


Figure 6. The streamlines for the flow between two parallel plates: (a) $Re = 20$; (b) $Re = 200$

flow. The lines of constant vorticity (Figure 10) are practically analogous to the data obtained by Morihara and Cheng.⁴⁰

The flow in a square cavity with driven upper lid

Although the calculations of the flow in the inlet section of the parallel plates show the stability and the convergence of the method, the absence of recirculating flows in these domains does not allow one to answer the question whether this scheme is stable or not. One of the types of flows which often serves as means for checking up numerical schemes is the circulating flow in a square cavity with a driven upper wall. Such a flow was calculated by BEM technique under the following boundary conditions:

on the fixed left, right and bottom walls

$$u_1 = u_2 = 0, \quad f' = 0, \quad \Psi = 0;$$

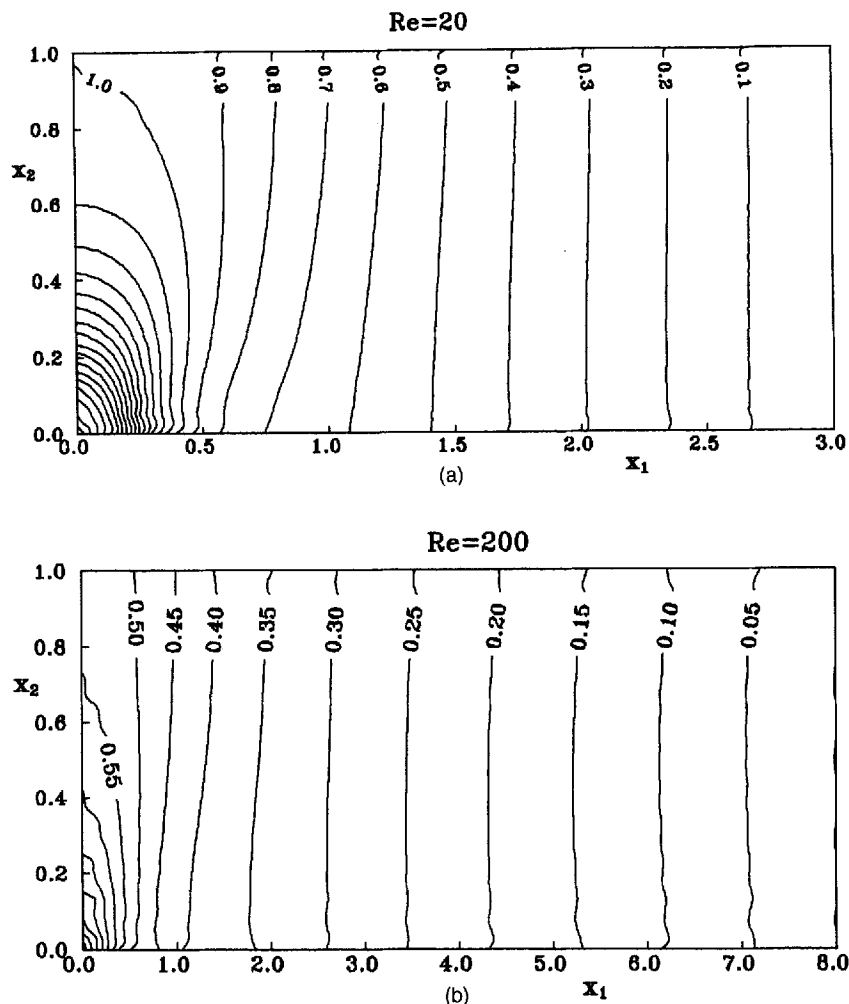


Figure 7. The pressure contours: (a) $Re=20$; (b) $Re=200$

on the translationally driven upper wall

$$u_1=1, \quad u_2=0, \quad f'=0, \quad \Psi=0.$$

The calculations were made for two Reynolds numbers $Re=1/\nu$ 1 and 100. In the first case a rather coarse mesh was used with 28 boundary elements and 98 equal triangular cells, and for $Re=100$ a finer mesh with 60 BEs and 450 equal triangular cells was used.

One of the peculiarities in calculating the flow in square cavity is the jump of velocity values u_1 in the cavity's left and right upper corners. The jump of this kind is not a physical one and may introduce some uncertainty in determining the boundary conditions, especially in FDM and FEM. Difficulties may arise while using linear and quadratic continuous BEs as well. The use of constant BEs permits one to overcome such uncertainty in the boundary conditions easily.

Another peculiarity of the numerical calculations of flow in a square cavity is the uncertainty in defining the field of pressure, which can be found only in a relative form. The absence of the part

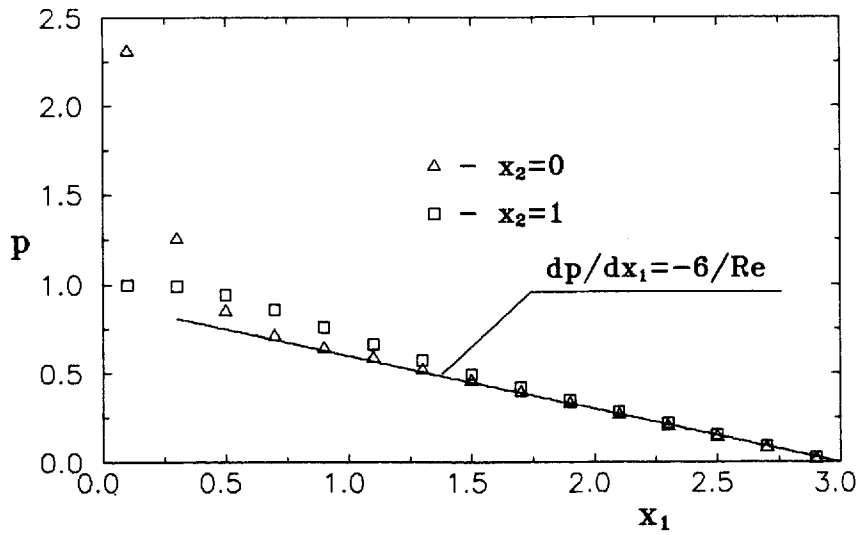


Figure 8. The pressure drop along the channel length for $Re=20$

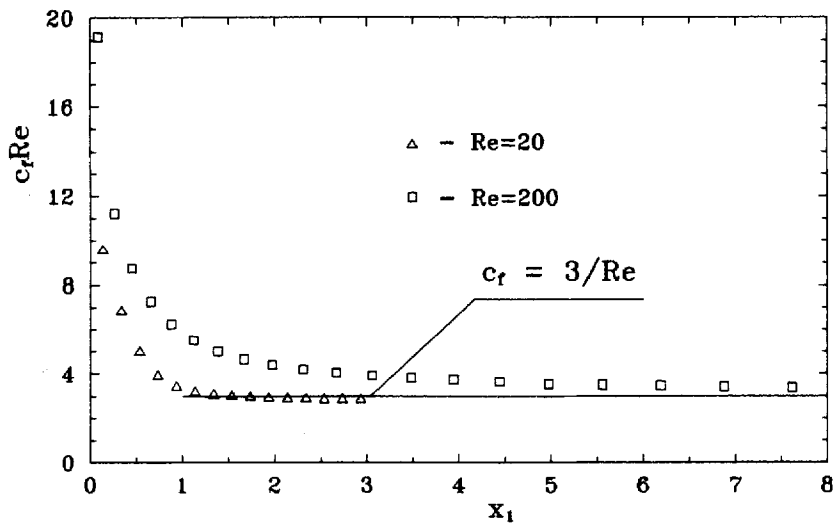


Figure 9. The friction coefficient development along the channel length

of boundary Γ_p does not permit one to find the absolute values of the pressure corrections p' and, consequently, the absolute pressure value p . Thus, the calculations were made at two different approaches to boundary conditions for p' and f' . In the first case, we took $f'_m=0$ for all BEs and the values of p'_m were found while solving the BIE (22). Then the relative pressure values at all nodes of calculation domain were determined as the difference between the calculated (absolute) pressures and the pressures at the centre of the lower wall. In the second case $x_1=0.5, x_2=0$ for the boundary node under the condition $p'=0; f'_m=0$ —for all other boundary nodes. In this

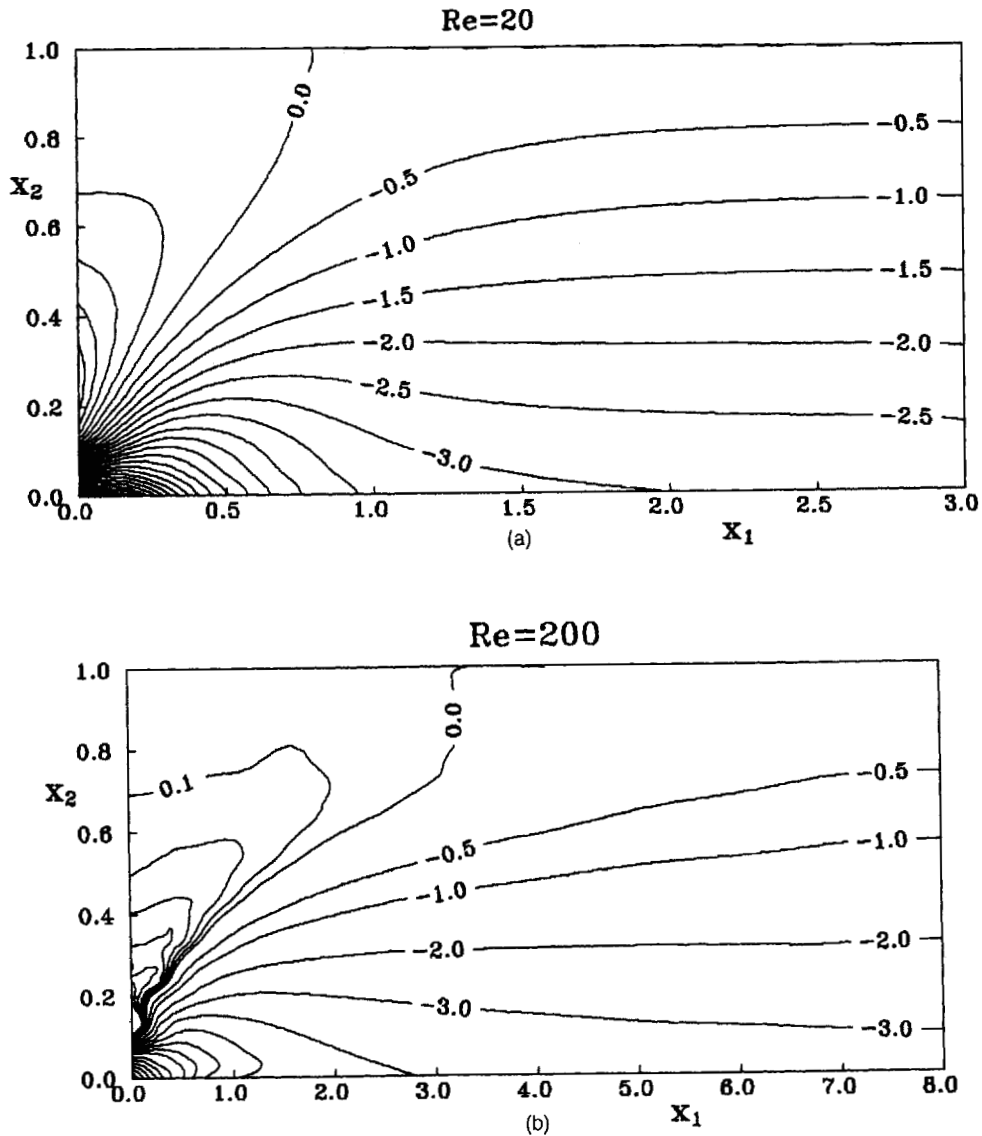
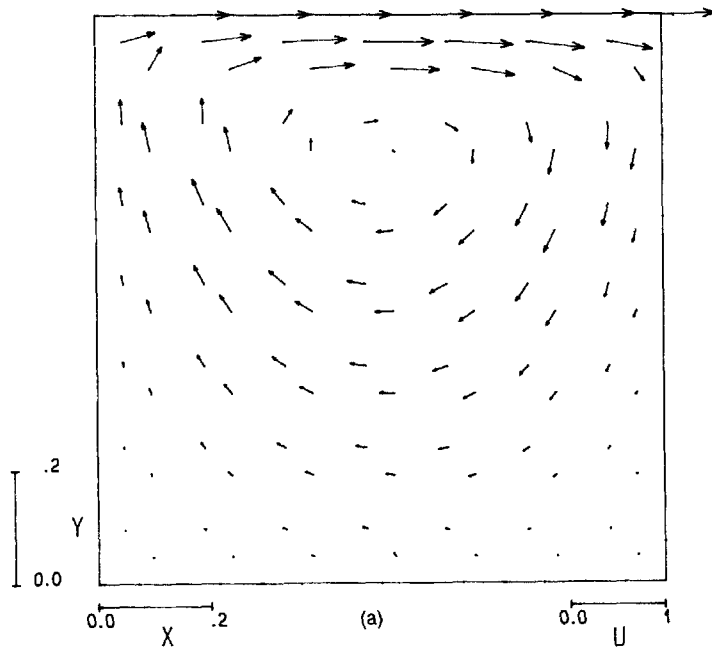


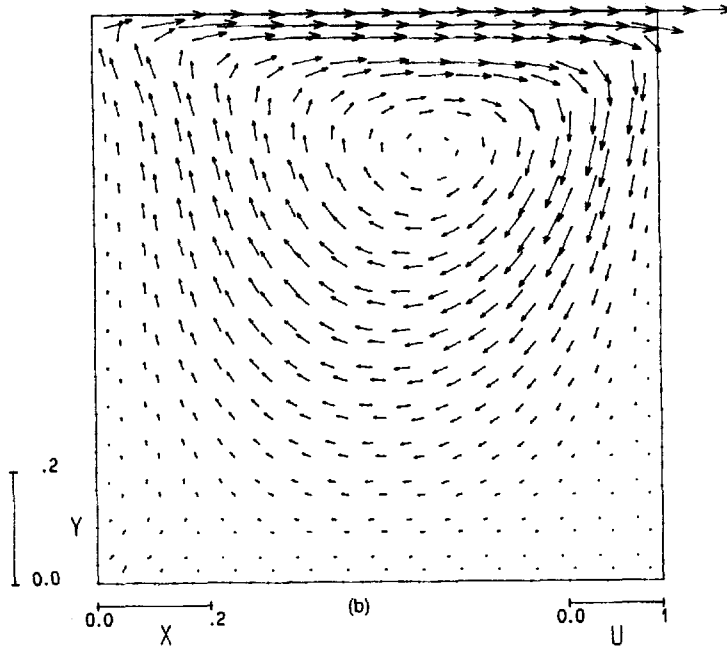
Figure 10. The vorticity contours: (a) $Re=20$; (b) $Re=200$

singular node, the velocity correction was not carried out naturally. This method has permitted us to obtain the absolute pressure values. Comparing the analysis of the solution results, obtained in two different ways, it became clear that both velocity fields and pressure fields were greatly alike.

Figures 11(a) and 11(b) show the calculated vector velocity fields at $Re=1$ and $Re=100$, respectively. The lines of the constant stream functions at $Re=1$ in Figure 12(a) are entirely analogous to the data of Sivaloganathan and Shaw.⁴¹ The vorticity centre is situated on the vertical symmetry axis of the cavity. With the growth of the Reynolds number, let the primary vortex move from the symmetry axis in the direction of the trajectory of the upper wall (Figure 12(b)). Although the streamlines' pattern coincides qualitatively with the data of Burgraff⁴² and



Driven Cavity Flow Field ($Re=1$)



Driven Cavity Flow Field ($Re=100$)

Figure 11. The vector velocity field for the flow in square driven cavity: (a) $Re=1$; (b) $Re=100$

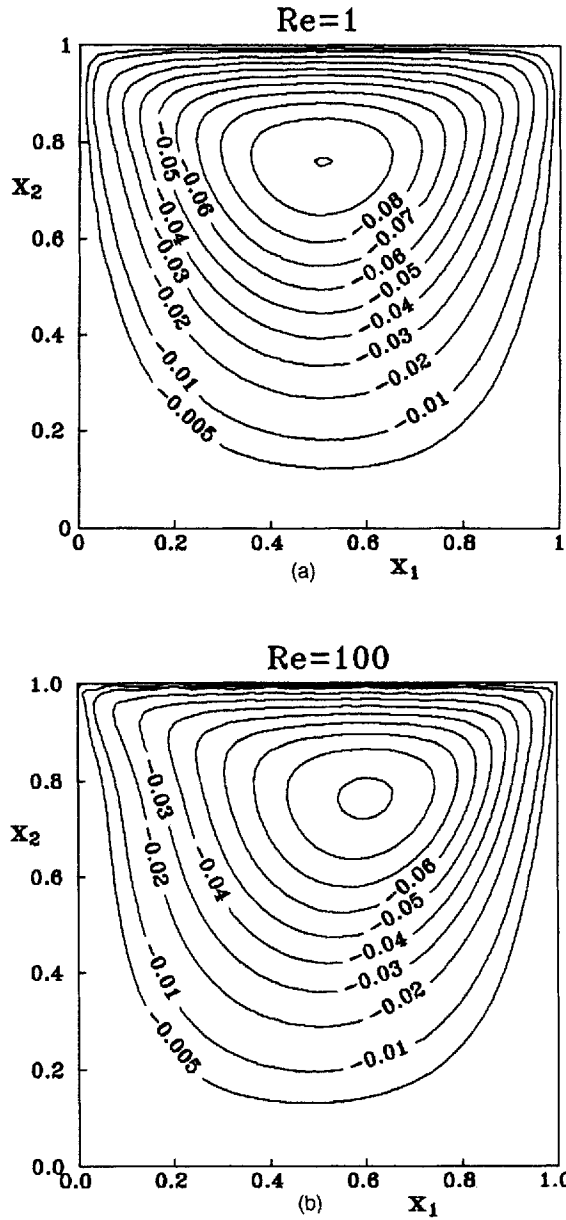


Figure 12. The streamlines for the flow in a square driven cavity: (a) $Re=1$; (b) $Re=100$

Mills,⁴³ the minimum stream function value is 9–10% higher than that obtained by other authors.^{42, 44–47} Some value of Ψ overstating in the vortex centre is caused by understating the values of the velocities u_1 at $0 \leq x_2 < 0.5$, taken along the vertical through the vortex centre (Figure 13).

The lines of constant vorticity (Figure 14(a)) and constant pressure (Figure 15(a)) at $Re=1$ are nearly fully symmetrical. These results correspond well with the known data.⁴¹ The vorticity field

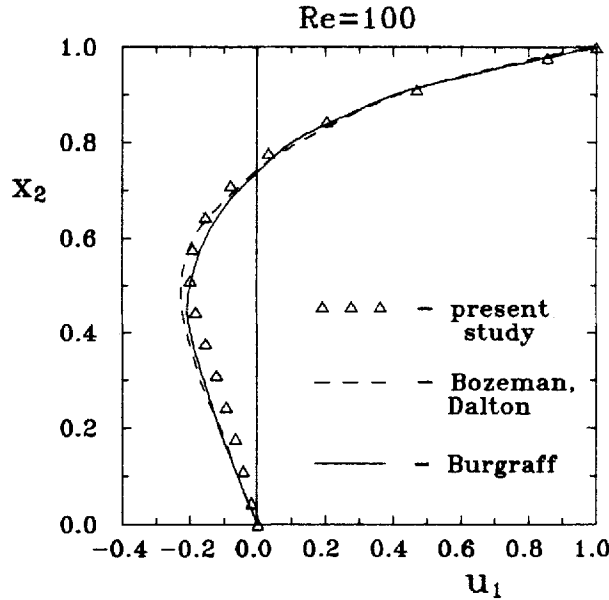


Figure 13. The vertical velocity profile along the vortex centre for the flow in a square driven cavity for $Re=100$

show a qualitative agreement (Figure 14(b)) with the results of References 42 and 46, and the pressure field shows a quantitative agreement with the results of References 42, 46, 48 at $Re=100$. The fields ω and the changes in p are concentrated near the upper corners.

It must be mentioned that the numerical calculations of this method were absolutely stable while using the under-relaxation (28); so, no other strategies were necessary. This point is most important because in the alternative methods, FDM and FEM, some special strategies must be used to improve the stability of the numerical scheme in the recirculating flows (for instance, using an upwind scheme).

The flow in a channel with sudden symmetric expansion

In conclusion, the flow in a plane channel with sudden symmetric expansion will be considered. Half-height of the channel before the expansion was $h=1/2$ and after the expansion $H=1$. The Reynolds number $Re=1/\nu$ was chosen equal to 46.6 to compare with the known data.^{47, 49} The boundary conditions for this problem have the following form:

on the channel wall the no-slip conditions are

$$u_1 = u_2 = 0, \quad \Psi = 0, \quad f' = 0;$$

on the axis symmetry of channel

$$\partial u_1 / \partial n = 0, \quad u_2 = 0, \quad \Psi = 1, \quad f' = 0;$$

in the narrow channel exit (i.e. at the place of sudden expansion) a parabolic profile of longitudinal velocity component

$$u_1 = \frac{3}{2h} \left(1 - \frac{y^2}{h^2} \right),$$

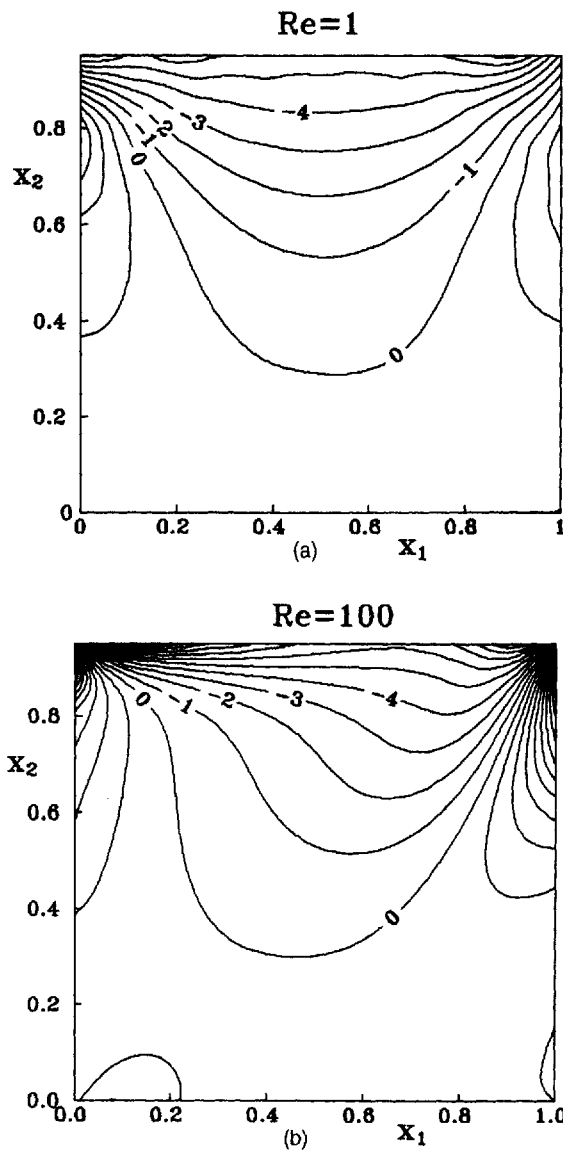


Figure 14. The lines of constant vorticity: (a) $Re=1$; (b) $Re=100$

where y is a co-ordinate measured from the symmetry axis,

$$\Psi = \frac{3}{2h} \left(y - \frac{y^3}{3h^2} \right), \quad f' = 0;$$

in the exit of the calculation domain

$$\frac{\partial u_1}{\partial n} = \frac{\partial u_2}{\partial n} = 0, \quad \frac{\partial \Psi}{\partial n} = 0, \quad p' = 0.$$

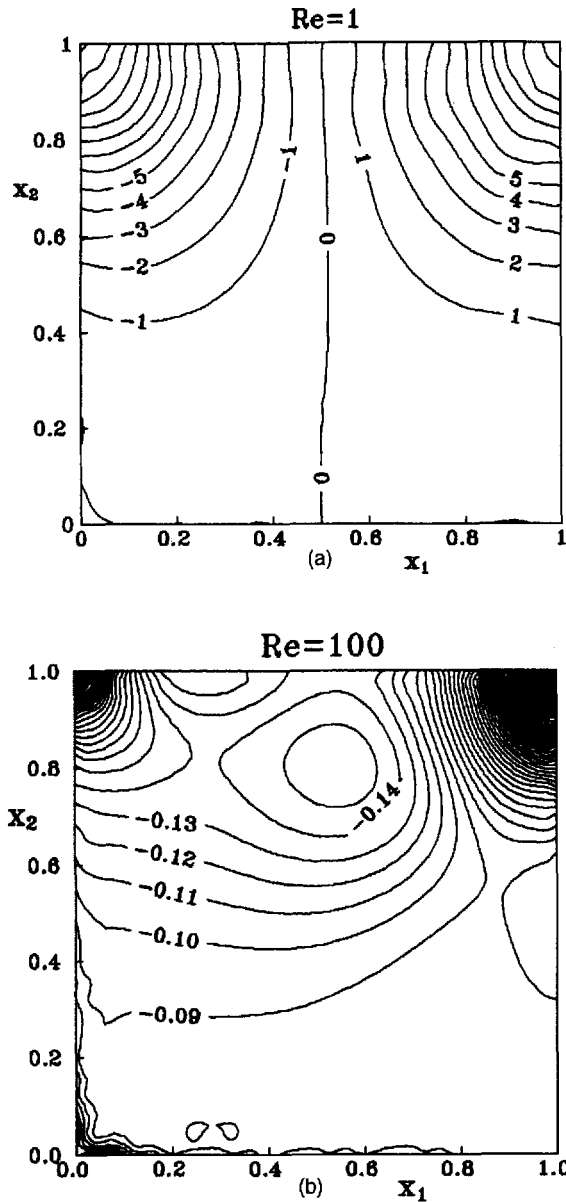
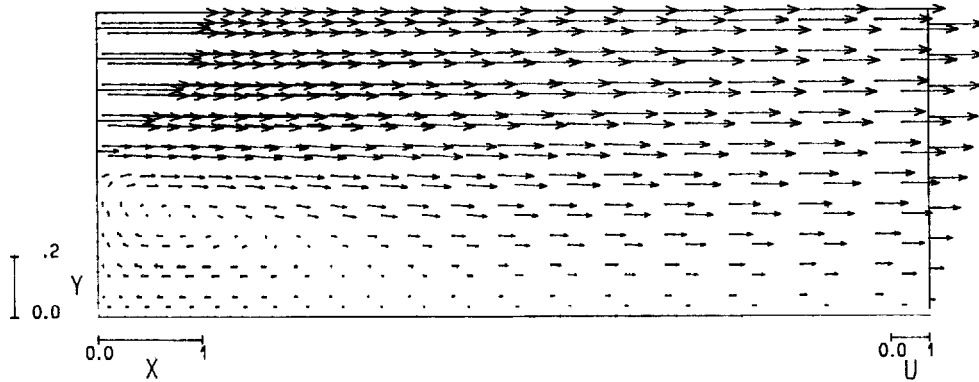


Figure 15. The pressure contours: (a) $Re=1$; (b) $Re=100$

The mesh used in BEM was the same as in the calculations of the flow in the inlet section of parallel plates at $Re=200$. The convergence of the solution for this problem was achieved in 210 iterations using the usual convergence criterion.

The vector velocity fields (Figure 16) demonstrate the recirculating region behind the step. The flow reattachment point is situated at $x_1/Re=0.060$ and, according to the results of References 47 and 49, the reattachment length is between 0.064 and 0.068. The minimum value of the stream



Flow Field in Channel with Sudden Simmetrical Expansion ($Re=46.6$)

Figure 16. The vector velocity field in the channel with sudden symmetric expansion

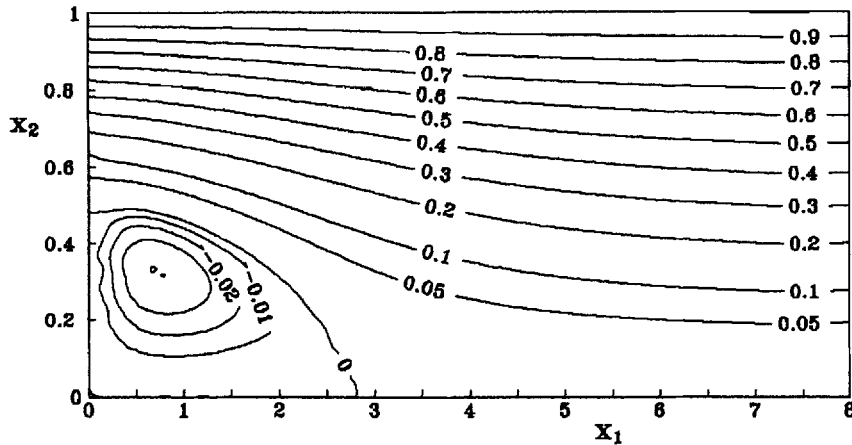


Figure 17. The streamlines

function at the recirculating region centre is $\Psi_m = -0.0405$ (Figure 17) and, according to the data of References 47 and 49, from -0.0444 to -0.045 .

Figure 18 shows the development of the streamwise velocity profiles. One can note that the character of the formation of velocity profiles is analogous to the results obtained by Agarwal.⁴⁷ Figure 19 shows the change of the velocities along the channel centreline. At $x_1/Re < 0.06$ the results conform well to the data of References 47 and 49, but downstream the disagreement increases because the length of the domain was chosen not long enough.

The main centre of vorticity generation in this flow is the step edge (Figure 20). A rather good agreement is observed in the changes of the vorticity on the channel lower wall (Figure 21), though at $x_1/Re > 0.1$ the value of vorticity according to BEM approaches the asymptotic value faster than for the calculated data of References 47 and 49. This is again connected with the choice of an inadequate length of the calculation domain.

This paper does not give calculations for rather large channel lengths because of the limited computer capacity. The implementation of the program, composed on the basis of this method

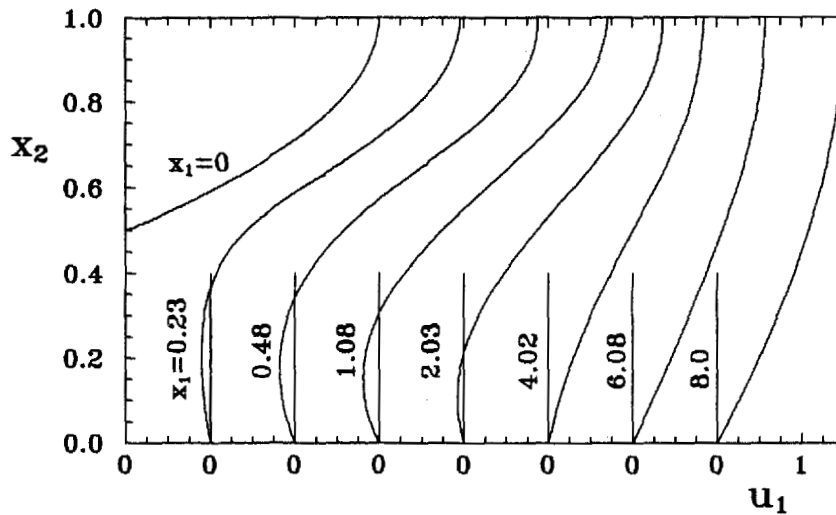


Figure 18. The development of the velocity profiles

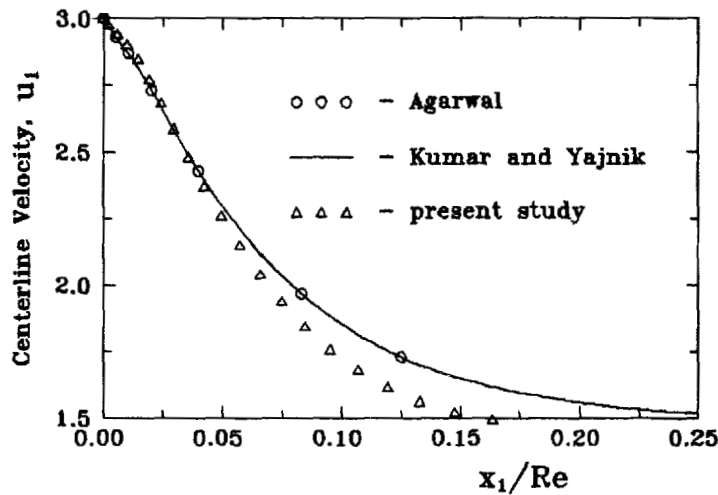


Figure 19. The velocity decay on the channel axis with sudden expansion

proved to be efficient only while using relatively short cells. It was shown that the ratio of right-angled triangle cathetus should not be higher than four. The use of longer cells does not converge the solution. It surely means that the real flow pattern is masked by the longer constant cells.

The pressure derivatives $\partial p/\partial x_2$ exist essentially only in the short inlet section (Figure 22), the main pressure changes taking place only along the x_1 co-ordinate.

The pressure value along the channel length changes non-monotonically (Figure 23). At sudden channel expansion, first the pressure value increases and then having reached its maximum at $x_1=5$ begins to decay according to the linear rule characteristic of the developed flow.

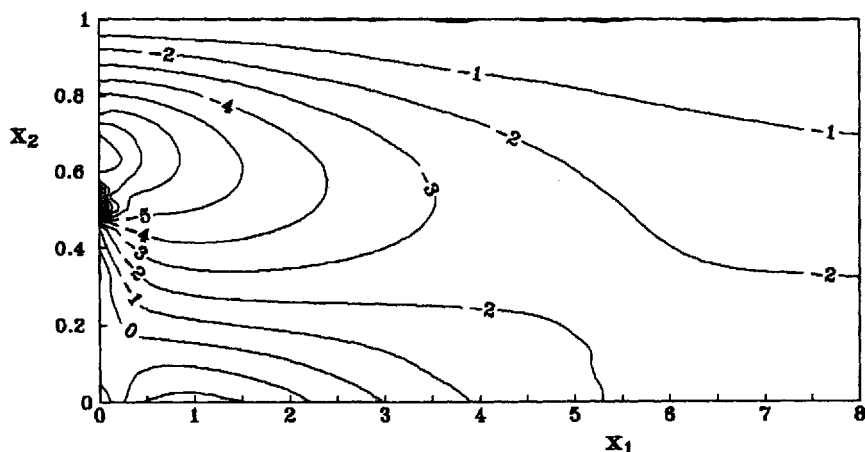


Figure 20. The vorticity contours

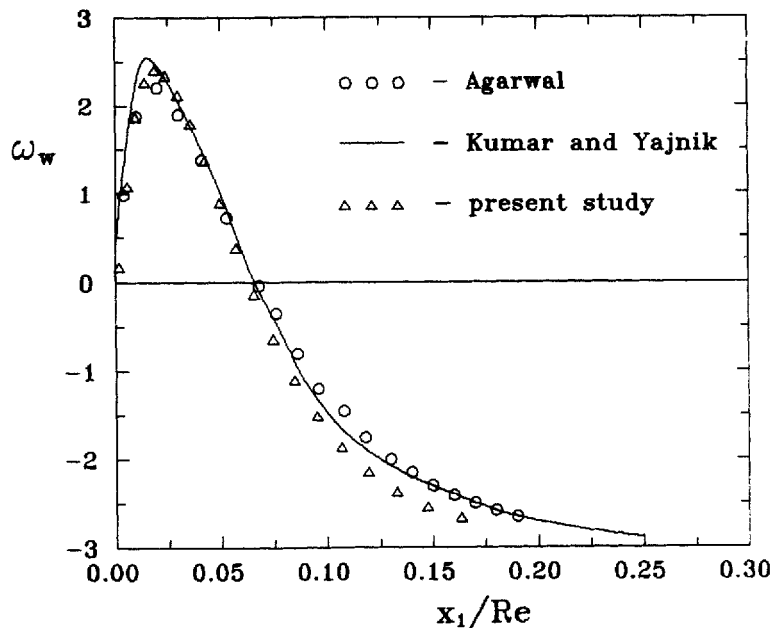


Figure 21. The development of vorticity on the channel wall

CONCLUSIONS

The paper describes a new numerical boundary element method for the steady incompressible laminar flow calculation. It is based on the widely known SIMPLE algorithm,³²⁻³⁴ which has been used successfully together with the control volume method for both laminar and turbulent flow calculations in the last 20 years. The method devised by the author permits one to determine the pressure and velocity corrections from the known fields of the velocity divergence without

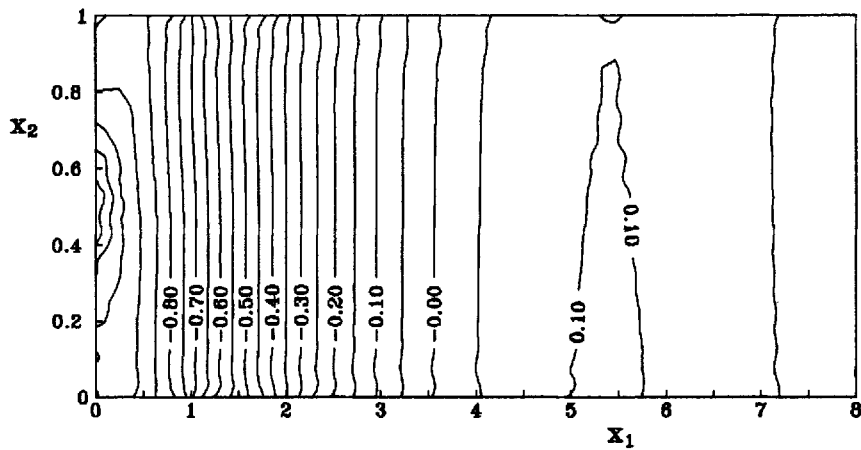


Figure 22. The constant pressure lines

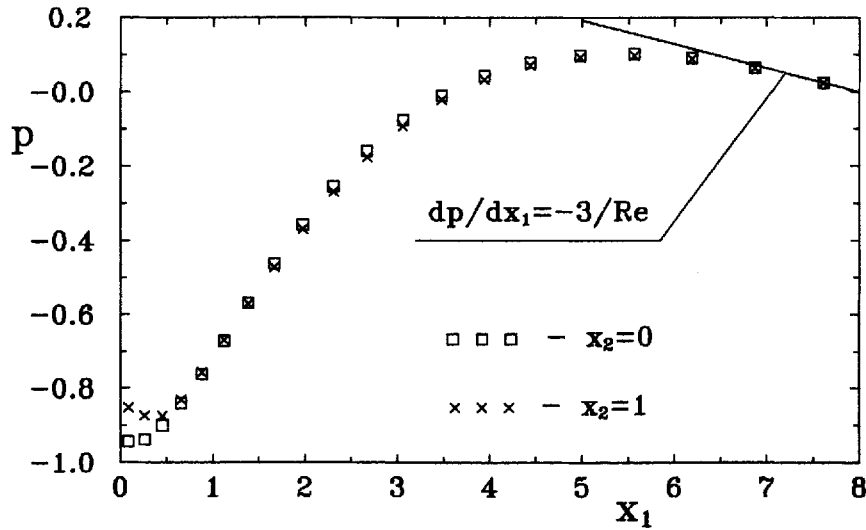


Figure 23. The development of pressure along the channel length

iterations. For the BIE discretization, constant boundary elements and constant triangular cells were used. The values of the integrals along the BE and cells were determined analytically (see Appendix). Discrete BIE for the source points on the boundary of the calculation domain were reduced to a system of linear algebraic equations, which were solved by the Gauss elimination method. The values of the velocities u_i and their derivatives $\partial u_i / \partial \xi_l$ were found in an explicit form from the given values of u_i , $\partial u_i / \partial n$ on the boundary Γ .

To achieve convergence of the solution, under-relaxation for the convection terms was used. The numerical calculations have shown the stability of this scheme for the recirculating flows as well. Excellent approximation was achieved at 80–240 iterations for the Reynolds numbers from 1 to 200.

The values of the vorticity and the stream function were found after obtaining the convergent solution for the values of the velocity derivatives $\partial u_i / \partial \xi_i$. The algorithm of their foundation was also based on the BEM technique.

The numerical calculation results for the following plane flows are presented:

- (a) in the inlet section of the parallel plates at $Re = 20$ and $Re = 200$;
- (b) in a square cavity with a driven upper lid at $Re = 1$ and $Re = 100$;
- (c) in a plane channel with sudden symmetric expansion at $Re = 46.6$.

A comparison of the results with the known data has shown the correctness of this numerical method.

The numerical solution method described here is based on the BEM technique and is applicable to both two-dimensional and three-dimensional steady incompressible viscous flows because of the formulae and equations (1)–(28) are identical for these flows. To solve the three-dimensional problems, alterations should be made for the calculations of vorticity and stream function and the evaluation of the discrete BIE coefficients (see the Appendix). One must take into account that the fundamental solution of the Laplace equation for three-dimensional problem has the form

$$u^* = \frac{1}{4\pi r},$$

and the boundary elements and volume cells will be considered, for instance, as triangles and tetrahedrons, respectively.

The proposed solution method is stable for calculating the separated and recirculating flows while using under-relaxation; so, no supplementary strategies are necessary (for instance, using an upwind scheme).

It is shown that the proposed method is efficient only while relatively short cells are used (the ratio of right-angled triangle cathetus should not be higher than four). The use of longer cells introduces instability in the numerical solutions, that essentially limits the applications of this BEM technique to solve the flow in channels with rather large length-to-height ratio.

This method seems to be developed for solving the unsteady viscous incompressible flows with the use of the fundamental solutions for unsteady diffusion equation. The use of this method to solve the incompressible turbulent flows is considerably limited because of the instability of this method at high Reynolds numbers.

It must be mentioned that the presented method allows one to solve the problems for domains of complex configuration without additional difficulties. This point is most important because in FDM there are considerable difficulties in the solution of the viscous flows in domains with complex configurations.

However, this method needs large computer storage for big arrays D_{km}^Ω , θ_{ikm}^Ω of the $N_c \times N_c$ and $2N_c \times N_c$ dimensions, respectively, and this limits significantly the use of this method on computers with relatively small storage. One of the ways to improve this method is to use the boundary elements and volume cells of a higher order together with the 'subdomain' method to reduce the computer consumption storage.

APPENDIX

For the two-dimensional domain the fundamental solution of the Laplace equation has the form

$$u^* = \frac{1}{2\pi} \ln \frac{1}{r}, \quad (36)$$

where

$$r = \sqrt{[(x_i - \xi_i)(x_i - \xi_i)]} \tag{37}$$

is the radius vector between the source and field points. All the integrals over the BEs and the cells have singularities at $r \rightarrow 0$ and, so they are likely to be found analytically.

The calculations of the contour integrals along the boundary elements are made according to the scheme given in Figure 24. The orthogonal co-ordinate system $z_1 \perp z_2$ is introduced, and it is strictly connected with the source point ξ , and the co-ordinate axis z_1 is orthogonal to the boundary element [1, 2].

The orthogonals e_1, e_2 of the auxiliary co-ordinate system are determined, respectively, as

$$e_{2i} = \frac{x_i^{(2)} - x_i^{(1)}}{L}, \quad e_{11} = e_{22}, \quad e_{12} = -e_{21}. \tag{38}$$

The integral over the n th BE

$$g(\xi) = \int_{\Gamma_j} u^*(\mathbf{x}, \xi) d\Gamma(\mathbf{x}) = -\frac{1}{2\pi} [z_2^{(2)}(\ln r_2 - 1) - z_2^{(1)}(\ln r_1 - 1) + h(\varphi_2 - \varphi_1)] \tag{39}$$

may be found analytically using the relations

$$z_2 = h \tan \varphi, \quad dz_2 = \frac{h d\varphi}{\cos^2 \varphi}, \quad r = \frac{h}{\cos \varphi},$$

where $z_2^{(1)} = h \times \tan \varphi_1, z_2^{(2)} = h \times \tan \varphi_2$ are the co-ordinates of the tops of the boundary elements (1) and (2), respectively, in the related co-ordinate system. When the source point approaches the boundary node, we will have from (39)

$$G_{mm} = \lim_{\xi \rightarrow \xi_m} g(\xi) = \frac{L_m}{2\pi} \left(1 - \ln \frac{L_m}{2} \right),$$

and the coefficients G_{jm}^Ω may be calculated directly from (39) on the condition that the tops of BEs (1), (2) and the point E form the counterclockwise contour direction. Otherwise, new numeration of the tops to achieve the desired triangle numeration 12E is introduced. The same procedure is fulfilled by the way for calculating the rest of the contour integrals.

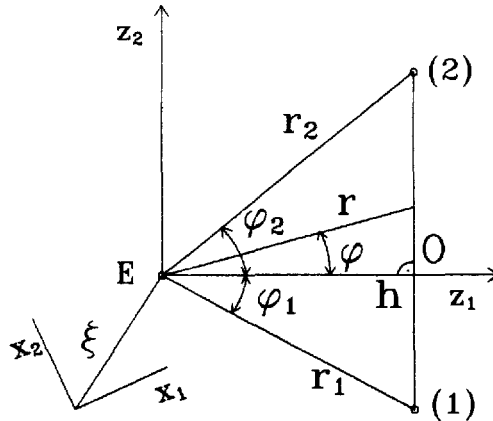


Figure 24. The co-ordinate system for analytical calculation of contour integrals

One must take into account

$$\frac{\partial u^*}{\partial \xi_l} = \frac{x_l - \xi_l}{2\pi r^2}, \quad \frac{\partial q^*}{\partial \xi_l} = \frac{n_l}{2\pi r^2} \frac{(x_l - \xi_l)n_l(x_l - \xi_l)}{\pi r^4}$$

for calculating the coefficients γ_{ljm}^Ω and β_{ljm}^Ω . From (20) the values of the integrals may be obtained:

$$\gamma_{ljm}^\Omega = \frac{1}{2\pi} \left[e_{1l}(\varphi_2 - \varphi_1) + e_{2l} \ln \frac{r_2}{r_1} \right], \quad (40)$$

$$\beta_{ljm}^\Omega = \frac{1}{2\pi} \left[\frac{e_{11}z_2^{(1)} - e_{21}h}{r_1^2} - \frac{e_{11}z_2^{(2)} - e_{21}h}{r_2^2} \right] \quad (41)$$

according to Figure 24.

To check the perfectness of γ_{ljm}^Ω calculations, the relation

$$\sum_{j=1}^{N_b} \gamma_{ljm}^\Omega n_{lj} = 1 \quad (42)$$

may be used. Relation (42) can be obtained in the following way. As the formula

$$\frac{\partial u^*}{\partial \xi_l} = - \frac{\partial u^*}{\partial x_l}$$

is valid, on discretizing the boundary integral

$$\int_{\Gamma} \frac{\partial u^*}{\partial n} d\Gamma = - \int_{\Gamma} \frac{\partial u^*}{\partial \xi_l} n_l d\Gamma$$

we obtain

$$\sum_{j=1}^{N_b} \gamma_{ljm}^\Omega n_{lj} \cong - \int_{\Gamma} \frac{\partial u^*}{\partial n} d\Gamma. \quad (43)$$

On the other hand,

$$\int_{\Gamma} \frac{\partial u^*}{\partial n} d\Gamma = \int_{\Omega} \nabla^2 u^* d\Omega \equiv -c_m \quad (44)$$

for the internal nodes $c_m = 1$; so, (42) is valid.

To check the perfectness of the coefficient β_{ljm}^Ω , let us transform the integral

$$\int_{\Gamma} \frac{\partial q^*}{\partial \xi_l} d\Gamma = \frac{\partial}{\partial \xi_l} \int_{\Gamma} q^* d\Gamma,$$

and taking into account (44), we have

$$\frac{\partial}{\partial \xi_l} \int_{\Gamma} q^* d\Gamma = 0.$$

So, the equality

$$\sum_{j=1}^{N_b} \beta_{ljm}^\Omega = 0 \quad (45)$$

is valid for $l = 1, 2, m = 1, 2, \dots, N_c$.

The value H_{mm} for the singular boundary elements equals zero, as the identity

$$(x_l - \xi_l)n_l = 0$$

is valid for the source point on BEs. While calculating \hat{H}_{jm} ($j \neq m$) and \hat{H}_{jm}^Ω , it is useful to note that

$$\hat{H}_{jm}^\Omega = - \sum_{l=1}^2 \gamma_{l(j)m}^\Omega n_{l(j)}. \tag{46}$$

So, taking into account that $n_l = e_{1l}$, $e_{1l}e_{2l} = 0$ and $e_{1l}e_{1l} = 1$ from (40) and (46), we have

$$\hat{H}_{jm}^\Omega = - \frac{\varphi_2 - \varphi_1}{2\pi}.$$

To check the perfectness of the calculations of \hat{H}_{jm} and \hat{H}_{jm}^Ω , one can use the relations

$$\sum_{j=1}^{N_b} \hat{H}_{jm} = -0.5, \quad \sum_{j=1}^{N_b} \hat{H}_{jm}^\Omega = -1.$$

The calculation of the integrals D_{km} by the cells does not present any special difficulties if the integral is offered as a sum (Figure 25),

$$\int_{\Omega_{123}} u^* d\Omega = \int_{\Omega_{12E}} u^* d\Omega + \int_{\Omega_{23E}} u^* d\Omega + \int_{\Omega_{13E}} u^* d\Omega, \tag{47}$$

and separate singular integrals over Ω_{12E} , Ω_{23E} , Ω_{13E} may be calculated by the scheme given in Figure 24. In this case the integral along any singular triangular cell has the form

$$\int_{\Delta} u^* d\Omega = - \frac{h^2}{4\pi} \left[\tan \varphi_2 \left(\ln r_2 - \frac{3}{2} \right) - \tan \varphi_1 \left(\ln r_1 - \frac{3}{2} \right) + \varphi_2 - \varphi_1 \right]. \tag{48}$$

The joint use of (47) and (48) dependencies suits the calculation of the integrals by the singular and by the regular cells as well. It is also important that the signs before the integrals in (47) are established 'automatically' only if the top numeration in triangles while calculating (48) is done counterclockwise. The values of the coefficients D_{km}^Ω may be calculated analogously from (47) and (48).

If we use the formula for the singular integral by the triangle cell then the values of the coefficients θ_{lkm}^Ω may be calculated from (47):

$$\int_{\Delta} \frac{\partial u^*}{\partial \xi_l} d\Omega = \frac{h}{2\pi} \left[e_{1l}(\varphi_2 - \varphi_1) + e_{2l} \ln \frac{\cos \varphi_1}{\cos \varphi_2} \right]. \tag{49}$$

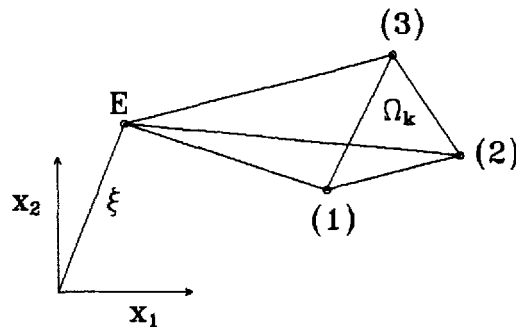


Figure 25. The description of integral calculations along the cells

It must be mentioned that though the values of the regular integrals by the BE and the cells can be found numerically using Gauss and Hammer methods, respectively,³ it is still preferable to evaluate them by the analytical relations obtained above.

REFERENCES

1. T. A. Cruse and R. B. Wilson, 'Advanced applications of boundary integral equation methods', *Nucl. Eng. Des.*, **46**, 223–234 (1978).
2. F. J. Rizzo and D. J. Shippy, 'An advanced boundary integral equation method for three-dimensional thermo-elasticity', *Int. j. numer. methods eng.*, **11**, 1753–1768 (1977).
3. C. A. Brebbia, J. C. F. Telles and L. C. Wrobel, *Boundary Element Techniques*, Springer, Berlin, 1984.
4. *BEASY (Boundary Element Analysis Systems) User's Manual*, Computational Mechanics Institute, Southampton, 1982.
5. J. C. Wu and M. M. Wahbah, 'Numerical solution of viscous flow equations using integral representations', in *Lecture Notes in Physics, Vol. 59*, 1976, pp. 448–453.
6. J. C. Wu and J. F. Thomson, 'Numerical solutions of time-dependent incompressible Navier–Stokes equations using an integro-differential formulation', *Comput. Fluids*, **1**, 197–215 (1973).
7. J. C. Wu, 'Fundamental solutions and numerical methods for flow problems', *Int. j. numer. methods fluids*, **4**, 185–201 (1984).
8. J. C. Wu, 'Boundary element solution of viscous flow problems', in C. A. Brebbia (ed.), *Boundary Element Technique: Applied Fluid Flow and Comput. Aspects. Proc. of Int. Conf.*, Rio de Janeiro, Springer-Verlag, Berlin, 1987, pp. 1–15.
9. P. Skerget, A. Alujevic and C. A. Brebbia, 'The solution of Navier–Stokes equations in terms of vorticity–velocity variables by boundary elements', in C. A. Brebbia (ed.), *Boundary Element Methods, Proc. 6th Int. Conf. on BEM*, C. M. Publications, 1984, pp. 4/41–4/56.
10. P. Skerget, A. Alujevic and C. A. Brebbia, 'Analysis of laminar flows with separation using BEM', in C. A. Brebbia and G. Maier (eds), *Boundary Elements Vol. 7, Proc. 7th Int. Conf. on BEM*, C. M. Publications, Southampton, 1985, pp. 9/23–9/36.
11. P. Skerget, A. Alujevic and C. A. Brebbia, 'Vorticity–velocity–pressure boundary integral formulation', in M. Tanaka and C. A. Brebbia (eds), *Boundary Elements Vol. 8, Proc. 8th Int. Conf. on BEM*, C. M. Publications, Southampton, 1986, Vol. 2, pp. 829–834.
12. P. Skerget, A. Alujevic, I. Zagar and G. Kuhn, 'Time dependent recirculation flow by the boundary element method', *ZAMM*, **69**, 270–272 (1989).
13. P. Skerget, A. Alujevic, C. A. Brebbia and G. Kuhn, 'Natural and forced convection simulation using the velocity–vorticity approach', in C. A. Brebbia (ed.), *Topics in Boundary Element Research. Vol. 5. Viscous Flow Applications*, C.M. Publications, Southampton, 1989, pp. 49–86.
14. S. C. R. Dennis and L. Quartapelle, 'Some uses of Green's theorem in solving the Navier–Stokes equations', *Int. j. numer. methods fluids*, **9**, 871–890 (1989).
15. H. A. Rodriguez-Prada, E. F. Pironti and A. E. Saez, 'Fundamental solution of the streamfunction–vorticity formulation of the Navier–Stokes equations', *Int. j. numer. methods fluids*, **10**, 1–12 (1990).
16. K. Kitagawa, C. A. Brebbia, L. C. Wrobel and M. Tanaka, 'Boundary element analysis of viscous flow by penalty function formulation', *Eng. Anal.*, **3**, 194–200 (1986).
17. K. Kitagawa, L. C. Wrobel, C. A. Brebbia and M. Tanaka, 'A boundary element formulation for natural convection problems', *Int. j. numer. methods fluids*, **8**, 139–144 (1988).
18. K. Kitagawa, C. A. Brebbia and M. Tanaka, 'A boundary element analysis for thermal convection', in C. A. Brebbia (ed.), *Topics in Boundary Element Research. Vol. 5, Viscous Flow Applications*, C.M. Publications, Southampton, 1989, pp. 87–109.
19. K. Kitagawa, 'Boundary element analysis of viscous flow', in *Lecture Notes in Engineering*, Springer, Berlin, 1990.
20. M. El-Refaee, 'Aerodynamics of airfoils in shear flows—a numerical study', in C. A. Brebbia and A. Chaudouet-Miranda (eds), *Boundary Elements in Mechanical and Electrical Engineering, Proc. Int. Bound. Elem. Symp.*, Nice, France, 1990, pp. 327–336.
21. C. V. Camp and G. S. Gipson, 'A boundary element method for viscous flows at low Reynolds numbers', *Eng. Anal. with Boundary Elements*, **6**, 144–151 (1989).
22. S. Sekar and G. Nath, 'Boundary element solution for Navier–Stokes equations in a constricted channel', *Acta Technica CSAV*, **35**, 620–641 (1990).
23. N. Tosaka, K. Kakuda and K. Onishi, 'Boundary element analysis of steady viscous flows based on P–U–V formulation', in C. A. Brebbia and G. Maier (eds), *Boundary Elements Vol. 7, Proc. 7th Int. Conf. on BEM*, C.M. Publications, Southampton, 1985, pp. 9/71–9/80.
24. A. D. Gosman and W. M. Pun, 'The TEACH program', in *HTS Course Notes*, Imperial College, London, 1974.
25. *FIDAP User's Manual*, Fluid Dynamics International, Evanston, IL, 1987.
26. J. C. Wu, C. M. Wang and U. Gulcat, 'Zonal solution of unsteady viscous flow problems', *AIAA Paper 84–1637*, 1984.
27. J. C. Wu, U. Gulcat, C. M. Wang and N. L. Sankar, 'A generalized formulation for unsteady viscous flow problems', in

- C. A. Brebbia (ed.), *Topics in Boundary Element Research. Vol. 5. Viscous Flow Applications*, C.M. Publications, Southampton, 1989, pp. 32–48.
28. P. Skerget, A. Alujevic, Z. Rek, I. Zagar, B. Namestnik and M. Hribersek, 'Boundary-domain integral method for the laminar and turbulent flow', in C. A. Brebbia and A. Chaudouet-Miranda (eds), *Boundary Elements in Mechanical and Electrical Engineering, Proc. Int. Bound. Elem. Symp.*, Nice, France, 1990, pp. 311–325.
 29. G. K. Youngren and A. Acrivos, 'Stokes flow past a particle of arbitrary shape: a numerical method of solution', *J. Fluid Mech.*, **69**, 377–403 (1975).
 30. C. Pozrikidis, 'A study of linearized oscillatory flow past particles by the boundary-integral method', *J. Fluid Mech.*, **202**, 17–41 (1989).
 31. O. A. Ladyzhenskaya, *The Mathematical Theory of Viscous Incompressible Flow*, Gordon & Breach, London, 1969.
 32. S. V. Patankar and D. B. Spalding, 'A calculation procedure for heat, mass and momentum transfer in three-dimensional parabolic flows', *Int. J. Heat Mass Transfer*, **15**, 1787–1806 (1972).
 33. S. V. Patankar, *Numerical Heat Transfer and Fluid Flow*, Hemisphere, Washington, DC, 1980.
 34. S. V. Patankar, 'A calculation procedure for two-dimensional elliptic situations', *Numer. Heat Transfer*, **4**, 409–425 (1981).
 35. H. Schlichting, 'Laminare kanaleinlaufstromung', *ZAMM*, **14**, 368–373 (1934).
 36. Y. L. Wang and P. A. Longwell, 'Laminar flow in the inlet section of parallel plates', *AIChE J.*, **10**, 323–329 (1964).
 37. J. Gillis and A. Brandt, 'The numerical integration of the equations of motion of a viscous fluid', *Air Force European Office of Aerospace Research Scientific Report 63-73*, 1964.
 38. J. W. McDonald, V. E. Denny and A. R. Mills, 'Numerical solutions of the Navier–Stokes equations in inlet regions', *ASME J. Appl. Mech.*, **39**, 873–878 (1972).
 39. A. Pollard and A. L.-W. Siu, 'The calculation of some laminar flows using various discretisation schemes', *Comput. Methods Appl. Mech. Eng.*, **35**, 293–313 (1982).
 40. H. Morihara and R.T.-S. Cheng, 'Numerical solution of the viscous flow in the entrance region of parallel plates', *J. Comput. Phys.*, **11**, 550–572 (1973).
 41. S. Sivaloganathan and G. J. Shaw, 'A multigrid method for recirculating flows', *Int. j. numer. methods fluids*, **8**, 417–440 (1988).
 42. O. R. Burgraff, 'Analytical and numerical studies of the structure of steady separated flows', *J. Fluid Mech.*, **24**, 113–151 (1966).
 43. R. D. Mills, 'Numerical solutions of the viscous flow equations for a class of closed flows', *J. Roy. Aeronaut. Soc.*, **69**, 714–718 (1965).
 44. M. M. Gupta and R. P. Manohar, 'Boundary approximations and accuracy in viscous flow computations', *J. Comput. Phys.*, **31**, 265–288 (1979).
 45. J. D. Bozeman and Ch. Dalton, 'Numerical study of viscous flow in a cavity', *J. Comput. Phys.*, **12**, 348–363 (1973).
 46. M. L. Mansour and A. Hamed, 'Implicit solution of the incompressible Navier–Stokes equations on a non-staggered grid', *J. Comput. Phys.*, **86**, 147–167 (1990).
 47. R. K. Agarwal, 'A third-order-accuracy upwind scheme for Navier–Stokes solutions at high Reynolds numbers', *AIAA Paper 81-0112*, 1981.
 48. F. Sotiropoulos and S. Abdallah, 'Coupled fully implicit solution procedure for the steady incompressible Navier–Stokes equations', *J. Comput. Phys.*, **87**, 328–348 (1990).
 49. A. Kumar and K. S. Yajnik, 'Separated flows at large Reynolds numbers', *J. Fluid Mech.*, **97**, 27–51 (1980).
 50. K. Onishi, T. Kuroki and M. Tanaka, 'An application of boundary element method to incompressible laminar viscous flows', *Eng. Anal.*, **1**, 122–127 (1984).